Appl Microbiol Biotechnol (2016) 100:10417–10428
DOI 10.1007/s00253-016-7704-4

A novel NADPH-dependent reductase of *Sulfobacillus acidophilus* TPY phenol hydroxylase: expression, characterization, and functional analysis

Meng Li[1,2] · **Wenbin Guo**[1,2] · **Xinhua Chen**[1,2,3]

Received: 19 May 2016 / Revised: 20 June 2016 / Accepted: 21 June 2016 / Published online: 4 July 2016

Abstract The reductase component (MhpP) of the *Sulfobacillus acidophilus* TPY multicomponent phenol hydroxylase exhibits only 40 % similarity to *Pseudomonas* sp. strain CF600 phenol hydroxylase reductase. Amino acid sequence alignment analysis revealed that four cysteine residues (*Cys*-X_4-*Cys*-X_2-*Cys*-$X_{29\text{-}35}$-*Cys*) are conserved in the N terminus of MhpP for [2Fe-2S] cluster binding, and two other motifs (*RXYS* and *GXXS*/*T*) are conserved in the C terminus for binding the isoalloxazine and phosphate groups of flavin adenine dinucleotide (FAD). Two motifs (*S*/*T*-*R* and *yXCGp*) responsible for binding to reduce nicotinamide adenine dinucleotide phosphate (NADPH) are also conserved in MhpP, although some residues differ. To confirm the function of this reductase, MhpP was heterologously expressed in *Escherichia coli* BL21(DE3) and purified. UV-visible spectroscopy and electron paramagnetic resonance spectroscopy revealed that MhpP contains a [2Fe-2S] cluster. MhpP mutants in which the four cysteine residues were substituted via site-directed mutagenesis lost the ability to bind the [2Fe-2S] cluster, resulting in a decrease in enzyme-specific oxidation of NADPH. Thin-layer chromatography revealed that MhpP contains FAD. Substrate specificity analyses confirmed that MhpP uses NADPH rather than NADH as an electron donor. MhpP oxidizes NADPH using cytochrome *c*, potassium ferricyanide, or nitro blue tetrazolium as an electron acceptor, with a specific activity of 1.7 ± 0.36, 0.78 ± 0.13, and 0.16 ± 0.06 U/mg, respectively. Thus, *S. acidophilus* TPY MhpP is a novel NADPH-dependent reductase component of phenol hydroxylase that utilizes FAD and a [2Fe-2S] cluster as cofactors.

Keywords NADPH-dependent reductase · Multicomponent phenol hydroxylase · *Sulfobacillus acidophilus* TPY · Heterologous expression

Meng Li and Wenbin Guo contributed equally to this work.

✉ Xinhua Chen
chenxinhua@tio.org.cn

[1] Key Laboratory of Marine Biogenetic Resources, Third Institute of Oceanography, State Oceanic Administration, Daxue Road 184, Xiamen 361005, People's Republic of China

[2] Fujian Collaborative Innovation Center for Exploitation and Utilization of Marine Biological Resources, Key Laboratory of Marine Genetic Resources of Fujian Province, Xiamen 361005, People's Republic of China

[3] Laboratory for Marine Biology and Biotechnology, Qingdao National Laboratory for Marine Science and Technology, Qingdao 266071, People's Republic of China

Introduction

Bacterial multicomponent monooxygenases (BMMs) are non-heme, dinuclear iron enzymes capable of using molecular oxygen to hydroxylate a variety of organic substrates, thus contributing to the biodegradation and biocatalysis of organic compounds (Notomista et al. 2003). The BMM family includes soluble methane monooxygenase (sMMO), toluene monooxygenase (ToMO), and phenol hydroxylase (PH). sMMOs have been characterized extensively by researchers using a range of spectroscopic, crystallographic, and kinetic methods (Chatwood et al. 2004; Merkx et al. 2001; Whittington and Lippard 2001). ToMOs, which hydroxylate a wide array of aromatic compounds, have garnered considerable research attention in recent years (Donadio et al. 2015).

PHs convert phenol into less toxic intermediates, and as members of the BMM family, multicomponent PHs are distinguished from monocomponent PHs (Kukor and Olsen 1992). Multicomponent PHs are complex proteins consisting of multiple polypeptides (Tinberg et al. 2011). The PH produced by *Pseudomonas* sp. strain CF600 is a well-known six-component enzyme (components designated P0 to P5) encoded by the *dmpKLMNOP* gene cluster (Shingler et al. 1992).

BMMs usually contain three common components: a 200–255 kDa dimeric hydroxylase, a 38–45 kDa reductase component, and a 10–16 kDa cofactor-less regulatory protein (Sazinsky and Lippard 2006). Although the carboxylate-bridged dinuclear iron center is in the hydroxylase component, many reports have demonstrated that efficient hydroxylation of substrates by BMMs is not possible without both the reductase and regulatory components, which physically interact with the hydroxylase component to modulate the hydroxylation activity (Liu et al. 1997; Sazinsky and Lippard 2006; Tinberg et al. 2011). The regulatory protein couples oxidation of NAD(P)H to hydroxylation of the organic substrate, a process that has been characterized in sMMO and PH (Qian et al. 1997; Shinohara et al. 1998; Wang et al. 2015). The reductase component is usually an flavin adenine dinucleotide (FAD)- and [2Fe-2S]-containing enzyme that transfers electrons from NAD(P)H to the di-iron sites of the terminal oxygenase via the [2Fe-2S] cluster and flavin prosthetic group. The reductases of PH, sMMO, and ToMO (namely, PHR, MMOR, and ToMO F, respectively) are reportedly a single protein, based on the characteristic spectra of the FAD and [2Fe-2S] cluster cofactors, and the ability to oxidize NAD(P)H and transfer reducing equivalents from NAD(P)H to the oxygenase component or artificial acceptors in vitro (Cafaro et al. 2002; Chatwood et al. 2004; Pessione et al. 1999).

Reductases containing both flavin and an [2Fe-2S] cluster as cofactors are also associated with many aromatic dioxygenases, such as the *Acinetobacter* sp. ADP1 benzoate 1,2-dioxygenase, *Pseudomonas putida* naphthalene dioxygenase, and *P. cepacia* phthalate dioxygenase (Correll et al. 1992; Haigler and Gibson 1990; Karlsson et al. 2002), all of which are multicomponent oxygenases that catalyze the initial oxidation of aromatic benzene rings. Based on the electron transport chain composition, bacterial aromatic dioxygenases are grouped into three classes, designated I–III (Mason and Cammack 1992). Class I includes two-component enzymes consisting of a reductase that contains flavin and a [2Fe-2S] cluster as well as a terminal oxygenase. Based on the type of flavin utilized by the reductase, further subdivisions include IA flavin mononucleotide (FMN) and IB FAD. In class II, FAD and [2Fe-2S] redox centers are located on separate proteins. Class III enzymes consist of three components: a reductase that contains both FAD and a [2Fe-2S] cluster, as in class IB enzymes, and another ferredoxin that is necessary for electron transfer to the third oxygenase component. The class IB benzoate 1,2-dioxygenase reductase (BenC) and class III naphthalene dioxygenase reductase (NdoR) are typical iron-sulfur flavoproteins that contain both a ferredoxin-like [2Fe-2S] domain and a ferredoxin-NAD(P)H-reductase (FNR)-like domain (Karlsson et al. 2002). Phthalate dioxygenase reductase (PDR) (Correll et al. 1992), a class IA enzyme that uses FMN as the flavin group, also contains a ferredoxin-like domain and an FNR-like domain in reverse positions compared with BenC and NdoR. These reductases play important roles in the electron transport chains of multicomponent enzyme systems.

Sulfobacillus acidophilus strain TPY, a gram-positive bacterium isolated from a deep-sea hydrothermal vent in the Pacific Ocean, is an acidophile and moderate thermophile, with an optimal growth temperature of approximately 50 °C and optimal growth pH of 1.8 (Li et al. 2011). *S. acidophilus* TPY can completely degrade 100 mg/L of phenol in 40 h at 45 °C and pH 1.8 via the *meta*-pathway (Zhou et al. 2016). Amino acid sequence homology analyses suggested that five genes (i.e., *mhpLMNOP*) encode the five components of PH. In order to clarify the function of PH, in the present study, the reductase component (PHR) encoded by the *mhpP* gene (genomic locus tag: TPY_0634; GenBank accession: CP002901.1) was expressed in *Escherichia coli* and then purified and characterized in detail.

Materials and methods

Bacterial strains and growth conditions

The bacterial strains used in this study are listed in Table 1. *S. acidophilus* TPY, isolated from a hydrothermal vent in the Pacific Ocean (12°42′29″N, 104°02′01″W; water depth 3083 m) was deposited in the China Center for Type Culture Collection (CCTCC) under accession number CCTCC M 2010203. *S. acidophilus* TPY was grown aerobically on medium for culturing *S. acidophilus* (SA medium, 3 g/L $[NH_4]_2SO_4$, 0.5 g/L K_2HPO_4, 0.5 g/L $MgSO_4$, 0.1 g/L KCl, 0.01 g/L $Ca[NO_3]_2$, 13.9 g/L $FeSO_4 \cdot 7\ H_2O$, and 0.2 g/L yeast extract) (Zhou et al. 2016). The initial pH of the medium was adjusted to 1.8. Bacteria were cultivated at 50 °C in 250-mL flasks containing 100 mL of SA medium on a shaker operated at 180 rev/min. *E. coli* strains were grown at 37 °C in Luria-Bertani (LB) medium or on LB agar plates supplemented with 100 μg/mL of ampicillin, if necessary.

Sequence alignment and phylogenetic analysis of MhpP

Alignment of the amino acid sequence of MhpP (GenBank: AEJ38832.1) encoded on the *S. acidophilus* TPY genome (CP002901.1) with sequences of other reductase components,

Table 1 Bacterial strains, plasmids, and primers used in this study

Strains/plasmids/primers	Relevant characteristics	Reference/Source
Strains		
Sulfobacillus acidophilus TPY	Gram-positive, acidophilic, moderately thermophilic, isolated from a hydrothermal vent in the Pacific Ocean (12.2′29″N, 104.2′01″W; water depth 3083 m)	(Li et al. 2011)
E. coli DH5α	F^-, Δ(*lacZYA-argF*)*U169*,*recA1*,*endA1*,*hsdR17*(rk^-,mk^+), *supE44*, *thi-1*, *gyrA*, *relA1*	Invitrogen
E. coli DH5α (pET-His-mhpP)	*E. coli* DH5α harboring plasmid pET-His-mhpP, Ap^r	This study
E. coli BL21 (DE3)	F^-,*ompT*, *hsdS*(rBB^- mB^-), *gal*, *dcm*(DE3)	Invitrogen
E. coli BL21 (DE3) (pET-His-mhpP)	*E. coli* BL21 (DE3) harboring plasmid pET-His-mhpP, Ap^r	This study
Plasmids		
pET-His	Expression vector, Ap^r, His-tag	TaKaRa
pET-His-mhpP	Plasmid pET-His harboring *mhpP* gene, Ap^r, His-tag	This study
Primers	Sequence (5′-3′)	Restriction site/codon change
mhpP	F: 5′-CGC*GGATCC*ATGGCATATCGCATTC-3′ R: 5′-CG*GCTAGC*TTAACGCCCCCGCCGGC-3′	*Bam*HI and *Nhe*I
C37A	F: 5′-TTGCCTCACGCGGCCACCCATGGTACCT-3′ R: 5′-AGGTACCATGGGTGGCCGCGTGAGGCAA-3′	TGC → GCC
C42A	F: 5′-CACCCATGGTACCGCCGGCACCTGTAAAG-3′ R: 5′-CTTTACAGGTGCCGGCGGTACCATGGGTG-3′	TGC → GCC
C45A	F: 5′-TACCTGCGGCACCGCTAAAGCCCAGGTG-3′ R: 5′-CACCTGGGCTTTAGCGGTGCCGCAGGTA-3	TGC → GCT
C77A	F: 5′-GGTATGCGCTGTTAGCCCAAGCCAAACCG-3′ R: 5′-CGGTTTGGCTTGGGCTAACAGCGCATACC-3′	TGC → GCC

*Bam*HI and *Nhe*I recognition sites are *underlined* and in *italics*. Base changes are *underlined*. All codon changes will result in substitution of cysteine with alanine

including BenC (*Acinetobacter* sp. ADP1 benzoate 1,2-dioxygenase reductase), P5 (*Pseudomonas* sp. CF600 phenol hydroxylase reductase), and ferredoxins and NADPH-ferredoxin reductases (FNRs), was performed using the DNAMAN program. A phylogenetic tree of reductase components of BMMs and dioxygenases was constructed using the neighbor-joining method with the MEGA 5 program.

Gene cloning and expression vector construction

The plasmids and primers used in this study are listed in Table 1. The *mhpP* gene was amplified from the *S. acidophilus* TPY genome using *Pfu* DNA polymerase (Transgene Biotech, Beijing, China). The resulting 1053-bp amplified gene fragment was flanked by *Bam*HI and *Nhe*I restriction sites, which were introduced using the *mhpP* forward and reverse primers, respectively. The amplified DNA fragment was purified from the PCR products using an E.Z.N.A.™ gel extraction kit (Omega Bio-Tek, USA). The gene fragment and pET-His plasmid were digested with the restriction enzymes *Bam*HI and *Nhe*I and ligated using T4 DNA ligase (Sangon Biotech, Shanghai, China). The resulting plasmid, pET-His-mhpP, was transformed into *E. coli* DH5α. Positive colonies were selected on LB plates containing ampicillin and confirmed by sequencing of the harbored plasmid. The recombinant plasmid pET-His-mhpP was then obtained from *E. coli* DH5α and transformed into *E. coli* BL21(DE3).

Recombinant protein expression and purification

Escherichia coli BL21(DE3) cells harboring the plasmid pET-His-mhpP were cultivated at 37 °C in 100 mL of LB medium containing 100 μg/mL ampicillin. Isopropyl-β-D-thiogalactoside (IPTG) was added to a final concentration of 0.2 mM when the OD_{600} reached 0.4–0.6. Cells were then cultivated at 28 °C for an additional 5–6 h, harvested by centrifugation at 6000×*g* for 10 min at 4 °C, suspended in binding buffer (20 mM sodium phosphate, 500 mM NaCl, 30 mM imidazole (pH 7.4)), and disrupted by sonication. After centrifugation (12,000×*g*, 15 min, 4 °C), insoluble debris was removed, and the supernatant containing the soluble protein was transferred to a Ni-affinity chromatography column (GE Healthcare) pre-equilibrated with binding buffer. The column was then washed extensively with three column volumes of binding buffer. Next, the bound protein was eluted with 5 mL of elution buffer (20 mM sodium phosphate, 500 mM NaCl,

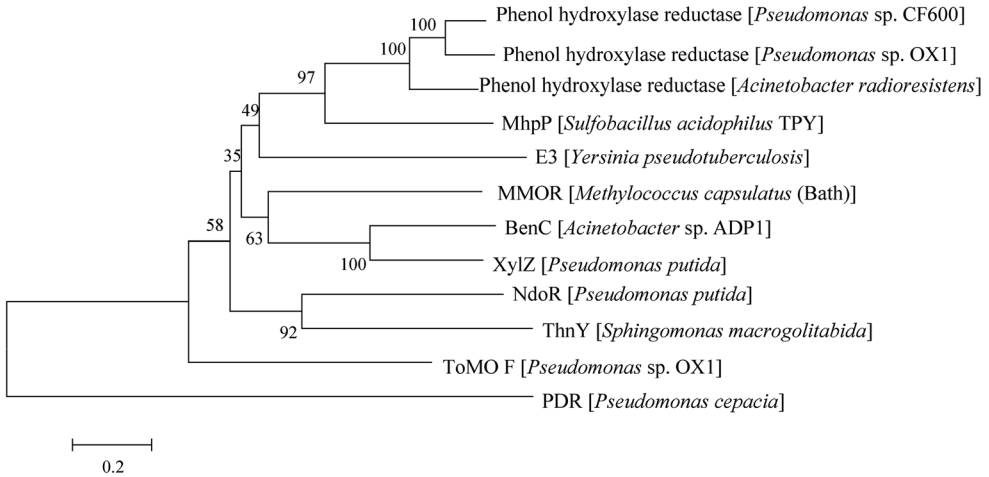

Fig. 1 Phylogenetic analysis of MhpP. *Pseudomonas* sp. strain CF600 phenol hydroxylase reductase (P19734.3); *Pseudomonas* sp. OX1 phenol hydroxylase reductase (AAO47360.1); *Acinetobacter radioresistens* phenol hydroxylase reductase (EEY87921.1). *E3 Yersinia pseudotuberculosis* CDP-6-deoxy-delta-3,4-glucoseen reductase (Q66DP5.3), *MMOR Methylococcus capsulatus* (Bath) soluble methane monooxygenase reductase (P22868.2), *BenC Acinetobacter* sp. ADP1 benzoate 1,2-dioxygenase reductase (CAG68302.1), *XylZ Pseudomonas putida* toluate 1,2-dioxygenase reductase (YP_003617181.1), *NdoR P. putida* naphthalene dioxygenase reductase (Q52126.1), *ThnY Sphingomonas macrogolitabida* tetralin biodegradation related iron-sulfur flavoprotein (AAU12856.1), *ToMOF Pseudomonas* sp. OX1 toluene monooxygenase reductase (CAD27360.1), *PDR Pseudomonas cepacia* phthalate dioxygenase reductase (AAB24396.1)

500 mM imidazole (pH 7.4)). Fractions containing the recombinant protein were collected and dialyzed at 4 °C against phosphate buffer (1.37 mM NaCl, 2.7 mM KCl, 10 mM $Na_2HPO_4{\cdot}12\ H_2O$, 2 mM KH_2PO_4, 5 % glycerol (pH 7.4)) to remove the imidazole. The recombinant protein was then concentrated by ultrafiltration and subjected to sodium dodecyl sulfate–polyacrylamide gel electrophoresis (SDS-PAGE, 12 % polyacrylamide) for visual estimation of molecular mass and purity. The protein concentration was determined using the Bradford assay (Bradford 1976).

Analysis of MhpP using UV-visible spectroscopy and electron paramagnetic resonance spectroscopy

The UV-visible absorption spectrum of purified MhpP (500 μg/mL) was measured from 190 to 800 nm using a Shimadzu UV-1800 spectrophotometer. Purified MhpP was also transferred into an electron paramagnetic resonance (EPR) quartz tube and frozen in liquid nitrogen for EPR determination. EPR spectra were recorded on a Bruker EMX-10/12 spectrometer equipped with a variable nitrogen temperature control system. Parameters were as follows: modulation frequency, 100 kHz; microwave power, 7 mW; modulation amplitude, 5 G; time constant, 20 ms, temperature, 90 K.

Identification of the MhpP flavin using UV-visible spectroscopy and thin-layer chromatography

Flavin was dissociated from recombinant MhpP by heating the protein at 100 °C for 5 min. The denatured protein was removed by centrifugation, and then the supernatant was analyzed using thin-layer chromatography (TLC) and UV-visible spectroscopy. The UV-visible spectra were recorded from 190 to 800 nm on a Shimadzu UV-1800 spectrophotometer (Shimadzu, Japan). TLC plates were developed with butanol/acetic acid/water (10:3:5). Commercial FAD and FMN (Sigma-Aldrich, USA) were used as standards, at a concentration of 50 μM. After development, the TLC plates were observed under 364-nm UV light.

Enzymatic activity assays

MhpP enzyme activity was assessed based on the oxidation of NADPH. Reactions were carried out at 25 °C in 200-μL mixtures containing 50 mM phosphate buffer (pH 7.4); 0.1 mM NADPH as an electron donor; 5 μg MhpP; various electron acceptors, including 0.1 mM bovine heart cytochrome *c*; 0.25 mM potassium ferricyanide; and 0.25 mM nitro blue tetrazolium. A mixture of all reaction components, except MhpP, was used as the negative control. The oxidation of NADPH and reduction of artificial electron acceptors by MhpP were assessed spectrophotometrically from 190 to

Fig. 2 Sequence alignment of MhpP with related proteins in the N-terminal [2Fe-2S]-binding domain (**a**), FAD-binding domain of the FNR-like region (**b**), and NAD(P)H-binding domain of the FNR-like region (**c**). Ferredoxin 1 and ferredoxin 2, ferredoxins from spinach and raphanus, respectively; *FNR 1, FNR 2,* and *FNR 3* NAD(P)H-ferredoxin reductase (FNR) from *Azotobacter vinelandii*, spinach and pea, respectively; *P5 Pseudomonas* sp. CF600 phenol hydroxylase reductase; *BenC Acinetobacter* sp. ADP1 benzoate 1,2-dioxygenase reductase. Conserved regions are shown in *boxes*. Residues indicated in *lowercase type* in the conserved motif *y-X-C-G-p* are comparatively less conserved; the Cys in this motif is substituted in MhpP ▶

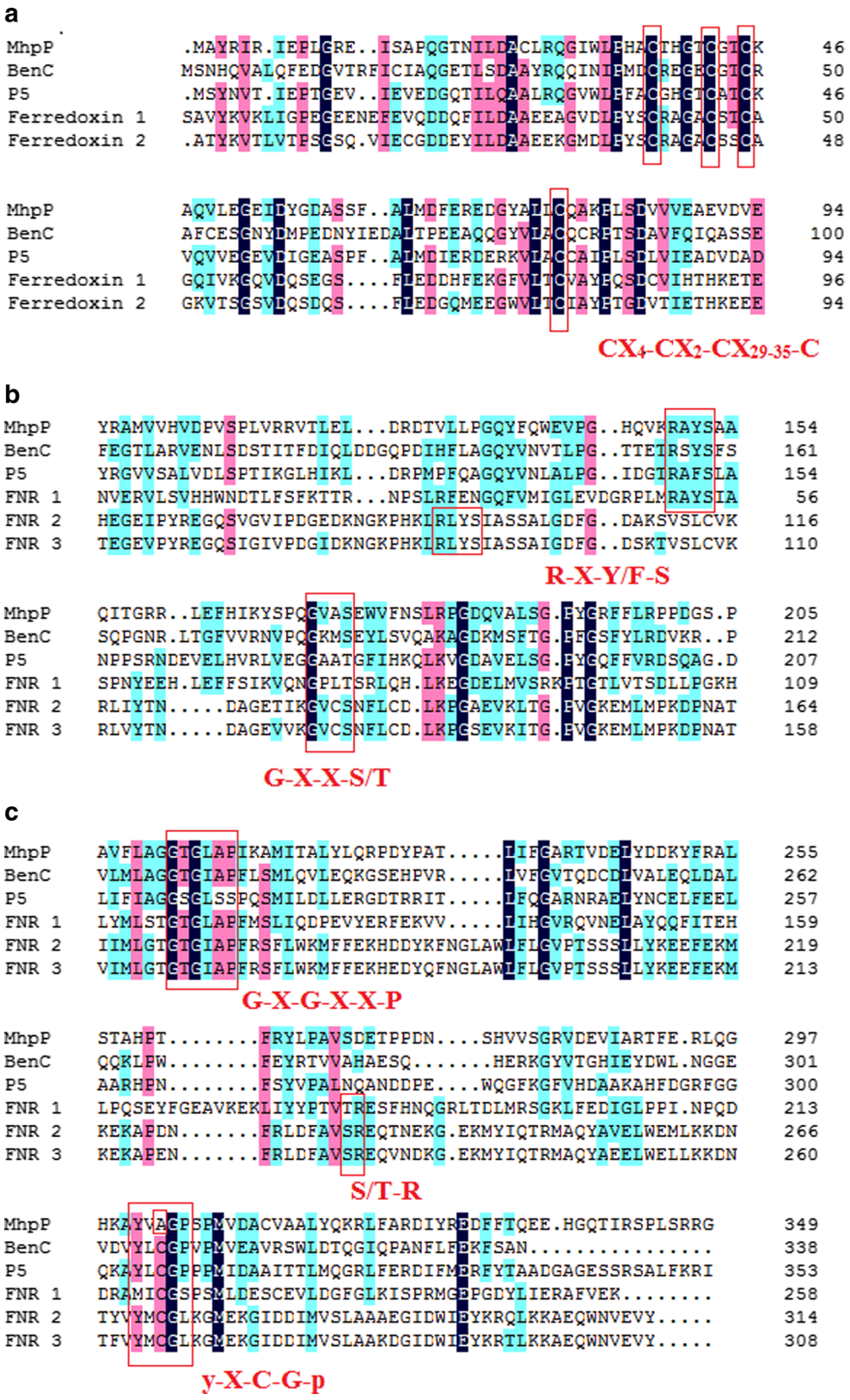

800 nm over time to evaluate changes in the characteristic absorption peaks of the artificial electron acceptors. Activity was assessed by monitoring changes at specific wavelengths using appropriate extinction coefficients: increase in absorbance at 550 nm for cytochrome *c* (ε_{550nm} = 21 mM^{-1} cm^{-1}), decrease in absorbance at 420 nm

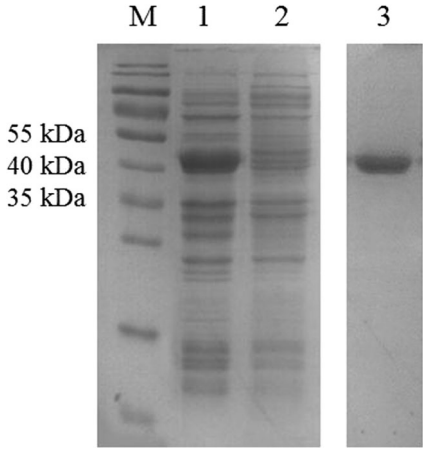

Fig. 3 SDS-PAGE analysis of MhpP. *M* molecular weight marker, *lane 1* the supernatant of *E. coli* BL21(pET-His-mhpP) after ultrasonication, *lane 2* the supernatant of *E. coli* BL21(pET-His) after ultrasonication, *lane 3* purified recombinant protein

for potassium ferricyanide (ε_{420nm} = 1.02 mM^{-1} cm^{-1}), and increase in absorbance at 550 nm for nitro blue tetrazolium (ε_{550nm} = 28 mM^{-1} cm^{-1}). The reactions were initiated by the addition of NADPH. One unit of MhpP activity was defined as the amount of enzyme required to reduce 1 μmol of electron acceptor per min at 25 °*C. Electron* donor preference was also investigated by adding NADH instead of NADPH to the reaction mixtures.

Site-directed mutagenesis of the gene encoding MhpP

In order to verify whether the cysteine residues of the *Cys-X_4-Cys-X_2-Cys-$X_{29–35}$-Cys* motif of MhpP are involved in binding the [2Fe-2S] cluster, site-directed mutagenesis of the gene encoding MhpP was carried out. The recombinant plasmid pET-His-mhpP was used as the template for constructing mutant-MhpP expression plasmids via PCR. The primers used for introducing the mutated sequences are listed in Table 1. PCR was performed using *Pfu* DNA polymerase with 15 cycles as follows: 30-s denaturation at 95 °C, 1-min annealing at 60 °C, and 5-min elongation at 72 °C, using an Eppendorf PCR cycler. After digestion with the restriction enzyme *Dpn*I to remove the template, the mutant-encoding plasmids were transformed into *E. coli* DH5α. Positive colonies were selected, and the harbored plasmids were sequenced to verify the presence of the desired mutations. Transformation of *E. coli* BL21(DE3) with the mutant-encoding plasmids and expression and purification of the mutant proteins were carried out according to the methods described above. Binding of MhpP mutants to the [2Fe-2S] cluster was assessed using UV-visible and EPR spectroscopy.

Results

Sequence homology analysis

Alignment of the amino acid sequences of MhpP and reductases of various multicomponent enzymes revealed 40 % similarity between MhpP and *Pseudomonas* sp. strain CF600 PH reductase (P5, GenBank: P19734.3) and 28 % similarity between MhpP and *Acinetobacter* sp. ADP1 BenC (CAG68302.1). Phylogenetic analyses revealed that MhpP is closely related to the PH reductases of a variety of species (Fig. 1). MhpP, P5, and BenC exhibited similar sequence length (about 330–350 amino acids) and two distinct N- and C-terminal conserved domains (Fig. 2). The N-terminal domain of MhpP was found to be similar to chloroplast-type ferredoxin, a small [2Fe-2S]-containing protein widespread in plants and bacteria, whereas the C-terminal domain was found to be similar to the FNR superfamily of flavoproteins, which contains FAD- and NAD(P)-binding motifs. In the N-terminal, chloroplast-type, ferredoxin-like region, four cysteine residues (arranged as *Cys-X_4-Cys-X_2-Cys-X_{29-35}-Cys*) were found to be conserved. These four cysteine residues correspond to C_{37}, C_{42}, C_{45}, and C_{77} of MhpP (Fig. 2a). In the C-terminal, motifs for binding isoalloxazine and phosphate

Table 2 Comparison of the characteristics of MhpP with those of other reductases of multicomponent oxygenases

Enzyme	Molecular mass (kDa)	Maximum absorption (nm)	Electron donor
MhpP	45	275, 348, 452, 492	NADPH
P5	41	275, 340, 430, 470	NADH
BenC	38	273, 340, 402, 467	NADH
NdoR	36	278, 340, 420, 460	NADH
TomoF	38	273, 335, 385, 454	NADH
MMOR	36	276, 340, 420, 480	NADH
PDR	36	275, 330, 420, 462	NADH

MMOR Methylococcus capsulatus (Bath) soluble methane monooxygenase reductase (P22868.2), *P5 Pseudomonas* sp. CF600 phenol hydroxylase reductase, *BenC Acinetobacter* sp. ADP1 benzoate 1,2-dioxygenase reductase (CAG68302.1), *NdoR Pseudomonas putida* naphthalene dioxygenase reductase (Q52126.1), *ToMO F Pseudomonas* sp. OX1 toluene monooxygenase reductase (CAD27360.1), *PDR Pseudomonas cepacia* phthalate dioxygenase reductase (AAB24396.1)

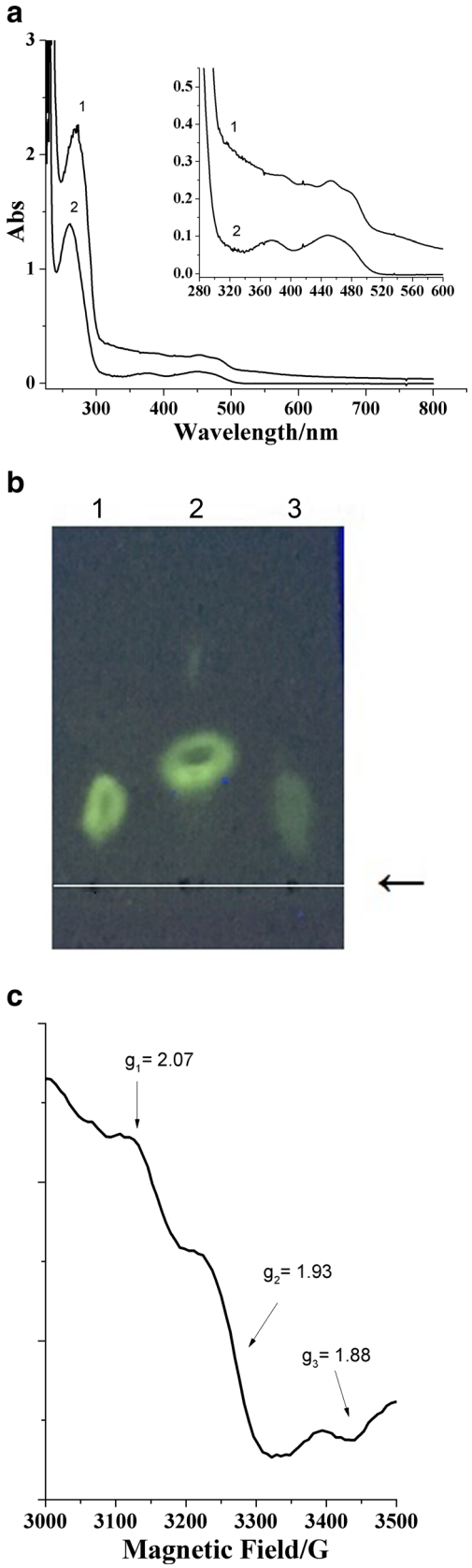

◀ **Fig. 4** UV-visible absorption spectrum (**a**), flavin identification via TLC (**b**), and EPR spectrum (**c**) of MhpP. **a** *Curve 1* UV-visible absorption spectrum of purified MhpP, *curve 2* UV-visible absorption spectrum of the protein-free supernatant obtained after boiling the protein solution for 5 min and centrifuging to remove the denatured protein precipitate. **b** *Lane 1* FAD standard solution, *lane 2* FMN standard solution, *lane 3* protein-free supernatant obtained after boiling the protein solution for 5 min and centrifuging to remove the denatured protein precipitate; *arrow* indicates the start development positions. **c** Reduced MhpP EPR spectrum of the [2Fe-2S] center, with g tensors of g_1 = 2.07, g_2 = 1.93, and g_3 = 1.88

groups of FAD (*RXY*/*FS* and *GXXS*/*T*) were conserved in MhpP and the reductase referring to (Fig. 2b). The *GXGXXP* motif, which is responsible for binding the pyrophosphate moiety of NAD(P), was also found to be conserved (Fig. 2c). Two conserved residues (*S*/*T*-*R*) were found to be present in FNR, but not in BenC and P5 (Fig. 2c). Although MhpP contains the conserved Ser, an Asp replaced the conserved Arg (Fig. 2c). The Cys residue in *yXCGp* motif of MhpP is substituted with an Ala residue (Fig. 2c).

Expression and purification of recombinant MhpP

After IPTG induction, MhpP was primarily present as soluble protein in the supernatant. The His-tagged recombinant protein was then purified by Ni-affinity chromatography. The eluate containing His-tagged MhpP was brownish yellow in color, indicating that the prosthetic groups were still bound to the protein. SDS-PAGE analysis revealed that the purified protein was pure, exhibiting a single 45-kDa band, consistent with the typical mass of bacterial oxygenase reductases (Fig. 3, Table 2).

Characterization of MhpP prosthetic groups

The UV-visible spectrum of purified MhpP showed absorbance peaks at around 275, 348, and 452 nm, with a shoulder at around 492 nm (Fig. 4a, curve 1). These absorbance peaks were attributed to the [2Fe-2S] center (absorbance maxima at about 340, 420, 470, and 540 nm) and flavin (absorbance maxima at about 280, 375 and 450 nm) bound to MhpP. The spectrophotometric features of MhpP were similar to those of other reductases of iron-sulfur flavoproteins (Table 2). MhpP was heated at 100 °C for 5 min, and the denatured protein precipitate was then removed. The absorbance maxima at 375 and 450 nm in the UV-visible spectrum of supernatant (Fig. 4a, curve 2) indicated that the flavin cofactor was non-covalently bound. TLC analysis indicated that the dissociated flavin was FAD, as the migration distance on the silica gel plate was identical to that of standard FAD rather than FMN (Fig. 4b). MhpP exhibited an EPR spectrum with g tensors of g_1 = 2.07, g_2 = 1.93 and g_3 = 1.88 (Fig. 4c), similar to those of the [2Fe-2S] center of plant-type ferredoxins, such as spinach ferredoxin (g_1 = 2.04, g_2 = 1.94, g_3 = 1.88) (Guigliarelli and Bertrand 1999). These data indicate that MhpP is an iron-

Table 3 Enzyme activity of wild-type and mutant MhpPs toward various electron acceptors

Electron acceptor	Enzyme specific activity (U/mg)					
	Wild-type		C37A	C42A	C45A	C77A
	NADPH	NADH	NADPH	NADPH	NADPH	NADPH
Cytochrome *c*	1.7 ± 0.36	0	0.54 ± 0.22	0.47 ± 0.17	0.64 ± 0.13	0.53 ± 0.16
Potassium ferricyanide	0.78 ± 0.13	0	0.63 ± 0.12	0.51 ± 0.09	0.48 ± 0.14	0.66 ± 0.11
Nitro blue tetrazolium	0.16 ± 0.06	0	0.12 ± 0.07	0.09 ± 0.05	0.07 ± 0.04	0.13 ± 0.08

sulfur flavoprotein containing FAD and an [2Fe-2S] cluster as cofactors.

NADPH is the preferred electron donor of MhpP

FNR-like iron-sulfur flavoproteins typically exhibit a preference for NADH and NADPH as electron donors. In this study, the ability of MhpP to use either NADH or NADPH as an electron donor was evaluated using cytochrome *c*, potassium ferricyanide, or nitro blue tetrazolium as the electron acceptor.

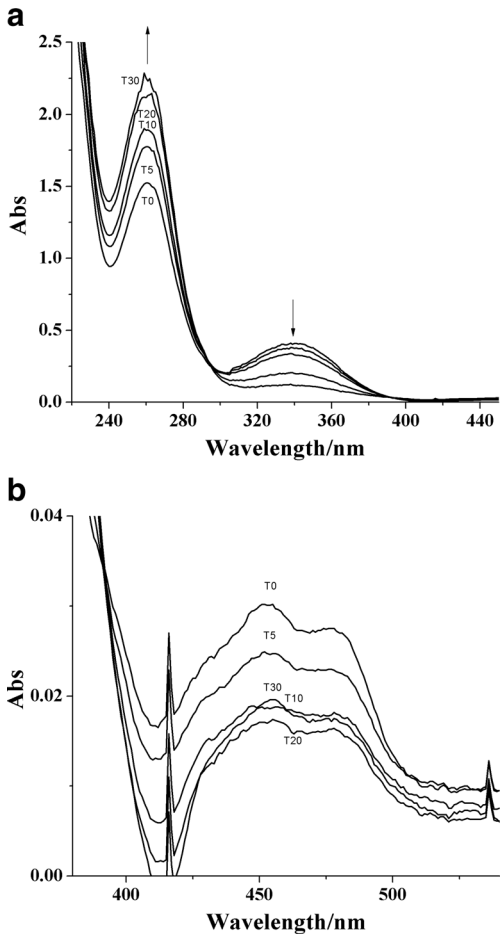

Fig. 5 UV-visible spectra of oxidation reaction mixtures containing NADPH and MhpP without addition of artificial acceptors revealing NADPH oxidation (**a**) and FAD (cofactor of MhpP) reduction (**b**). *T0–T30* indicate the reaction time 0–30 min

MhpP exhibited no electron transfer when NADH was used as the electron donor, but high electron transfer activity was observed with NADPH as the electron donor (Table 3). These results indicate that MhpP is an NADPH-dependent reductase, in contrast to P5 (Powlowski and Shingler 1990), MMOR (Nakajima et al. 1992), ToMO F (Cafaro et al. 2002), BenC (Yamaguchi and Fujisawa 1978), and NdoR (Haigler and Gibson 1990), all of which prefer NADH as the electron donor (Table 2). Changes in the absorption peaks of UV-visible spectra were monitored during the oxidation of NADPH by MhpP. As shown in Fig. 5a, the characteristic absorption of the reduced form, NADPH, decreased at 340 nm, whereas absorption of the oxidized form, $NADP^+$, increased at 260 nm over the course of the reaction (30 min). Figure 5b showed the absorbance at 450 nm contributed by FAD from MhpP over the course of the reaction (30 min). FAD reduction was observed in the first 20 min that absorbance at 450 nm was decreased. At the end of the reaction, the speed of re-oxidation of FAD prosthetic group under the aerobic condition was over the reduction that the absorbance at 450 nm recovered.

Analysis of MhpP catalytic activity using artificial electron acceptors

Reductases in multicomponent oxygenase systems transfer reducing equivalents from NAD(P)H to the catalytic site of terminal hydroxylases. In the presence of NAD(P)H, electrons can also be transferred in vitro to exogenous acceptors, such as potassium ferricyanide, nitro blue tetrazolium, or cytochrome *c*. In this study, changes in the absorbance of these exogenous electron acceptors over time were monitored spectrophotometrically. Progressive changes in the spectral properties of potassium ferricyanide, with an absorbance decrease at 420 nm, indicated that MhpP reduced potassium ferricyanide to potassium ferrocyanide (Fig. 6a). An increase in the characteristic absorption peak at around 550 nm indicted that nitro blue tetrazolium was reduced to insoluble formazan (Fig. 6b). The color of the reaction mixture containing nitro blue tetrazolium changed from yellow to purple. Obvious changes of peak intensity occurred at three wavelengths for cytochrome *c* (530 nm for the oxidized form; 520 and 550 nm for the

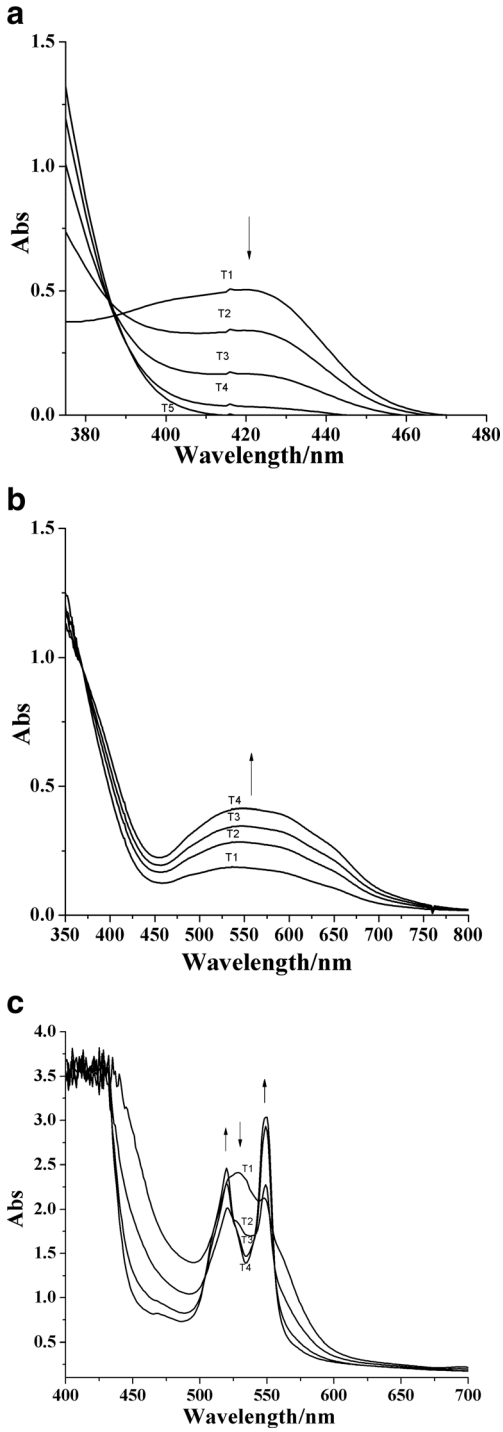

Fig. 6 UV-visible spectra of oxidation reaction mixtures containing NADPH and MhpP with potassium ferricyanide (**a**), nitro blue tetrazolium (**b**), cytochrome *c*, (**c**) as electron acceptors. *T1–T4* indicate the reaction time 1–4 min

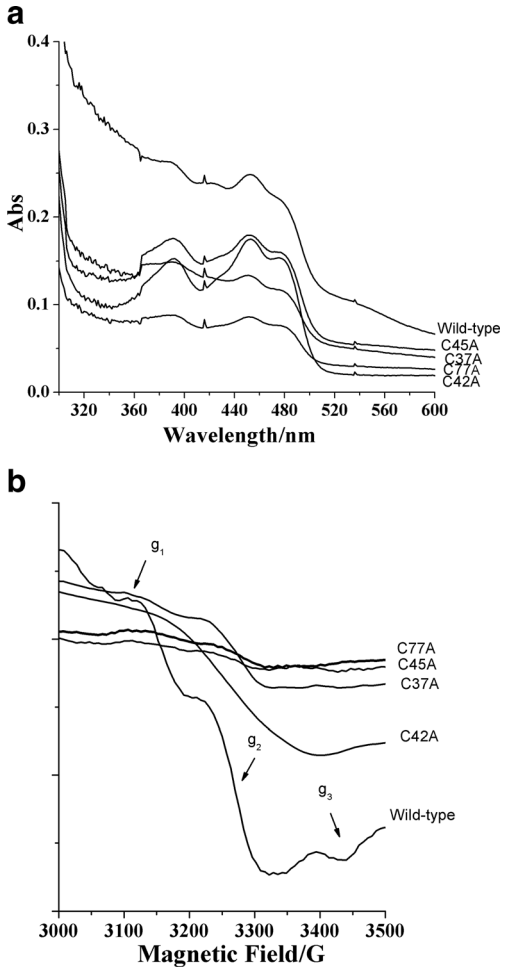

Fig. 7 UV-visible absorption spectra (**a**) and EPR spectra (**b**) of MhpP mutants

reduced form) during reduction of cytochrome *c* by MhpP (Fig. 6c). Table 3 lists the specific activity of MhpP with respect to these three electron acceptors. MhpP exhibited a specific activity of 1.7 ± 0.36 U/mg when cytochrome *c* served as the electron acceptor, which was higher than that observed when potassium ferricyanide (0.78 ± 0.13 U/mg) or nitro blue tetrazolium (0.16 ± 0.06 U/mg) were used, indicating that cytochrome *c* is a more suitable electron acceptor for MhpP.

Substitution of MhpP conserved Cys residues via site-directed mutagenesis

Sequence alignment analyses showed that the N-terminal domain of MhpP contains four highly conserved Cys residues (*Cys-X*$_4$*-Cys-X*$_2$*-Cys-X*$_{29\text{-}35}$*-Cys*) (Fig. 2a). These residues form the classic [2Fe-2S]-binding domain of ferredoxin family enzymes. Site-directed mutagenesis of the gene encoding MhpP was carried out to evaluate the role of these Cys residues. Sequencing of the mutant plasmids showed that all of them carried the target mutations. The mutant plasmids were then transformed into *E. coli* BL21(DE3), and the MhpP mutants were expressed and purified as soluble proteins. UV-visible spectra showed that the absorbance associated with the [2Fe-2S] cluster at around 340 and 540 nm was lower in the mutant proteins compared with wild-type MhpP (Fig. 7a).

Analysis of EPR spectra of the mutants confirmed that binding of the [2Fe-2S] clusters was impacted, as the characteristic g tensors were lost (Fig. 7b). These data confirm that the conserved Cys residues mediate binding of the [2Fe-2S] cluster in the ferredoxin-like domain of MhpP. The specific activities of the MhpP mutants toward the three artificial electron acceptors are shown in Table 3. The activity of the MhpP mutants toward potassium ferricyanide and nitro blue tetrazolium was 43.7–84.6 % of that of wild-type MhpP, whereas the activity toward cytochrome *c* was only about 27.6–37.6 % of that of wild-type MhpP. The lower specific activity of the mutant enzymes indicates that replacement of the conserved Cys residues affects binding of the iron-sulfur cluster, in turn affecting electron transfer between MhpP and its substrates.

Discussion

The N-terminal domain of MhpP contains four highly conserved cysteine residues (*Cys-X_4-Cys-X_2-Cys-X_{29-35}-Cys*) involved in [2Fe-2S]-cluster binding. These residues are important for maintaining the structure and function of the ferredoxin-like region and binding plant-type [2Fe-2S] clusters (Karlsson et al. 2002). UV-visible and EPR spectroscopy revealed that MhpP contains a [2Fe-2S] cluster (Fig. 4a, c). Replacement of the conserved Cys residues via site-directed mutagenesis resulted in loss of [2Fe-2S] cluster binding and a decrease in NADPH oxidation specific activity (Fig. 7; Table 3). This result was in line with analyses of Cys mutants of *Acidithiobacillus ferrooxidans* ferredoxin, which loses both the maxima contributed by the iron-sulfur cluster in UV-visible spectra and the specific g tensors in the EPR spectra (Jia et al. 2007). Previous analyses of the crystal structure of BenC indicated that the main-chain nitrogen atoms of these residues form hydrogen bonds with the sulfur and iron atoms in the [2Fe-2S] cluster (Karlsson et al. 2002). The specific enzyme activities of the four Cys mutants of MhpP varied, indicating that each of these four cysteine residues has different influence on the [2Fe-2S] cluster binding. The specific enzyme activity of C42A mutant was affected more greatly than the other three mutants (Table 3). This result was in accordance with the Cys mutants of an iron-sulfur flavoprotein ThnY, where the second Cys residue in the *Cys-X_4-Cys-X_2-Cys-X_{29-35}-Cys* domain was more important than the first one (Laura et al. 2013).

The C-terminal domain of MhpP contains conserved motifs (*RXYS* and *GXXS/T*) involved in binding the isoalloxazine and phosphate groups of FAD (Fig. 2b). TLC analyses revealed that MhpP contains FAD (Fig. 4b). Two motifs (*S/T-R* and *yXCGp*) responsible for binding NADPH are also conserved in MhpP, although some residues differ (Fig. 2c). These motifs are the characteristic signature of FNR family enzymes (Ceccarelli et al. 2004). In FNR, these two residues (*S/T-R*) interact with the 2′-phospho AMP moiety of $NADP^+$ (Karplus and Daniels 1991) and are therefore largely responsible for the selectivity for $NADP^+$ over NAD^+. In NAD^+-binding proteins such as PDR, Asp replaces the Ser and forms a hydrogen bond with the 2′-OH group, thus contributing to NADH specificity (Correll et al. 1993). The Cys residue in the *yXCGp* motif is conserved in almost all FNR family and FNR-like proteins (Ceccarelli et al. 2004; Correll et al. 1993; Shirabe et al. 1991). However, in MhpP, this Cys residue is substituted with an Ala residue (Fig. 2c). This Cys is reportedly involved in binding the nicotinamide moiety of NAD(P)H (Correll et al. 1993; Karplus and Bruns 1994). The natural substitution of this conserved Cys residue observed in MhpP is rare in FNR and FNR-like proteins. However, natural loss of the highly conserved Cys of *yXCGp* was reported for an iron-sulfur flavoprotein involved in tetralin biodegradation (García et al. 2011). Substrate specificity analyses confirmed that MhpP preferentially utilizes NADPH rather that NADH as an electron donor (Table 3). This preference for NADPH is consistent with the sequence alignment results, which indicated that the conserved Ser residue in the *S/T-R* motif of MhpP is responsible for binding NADPH.

According to the criteria of the multicomponent oxygenase classification system (Mason and Cammack 1992), MhpP is similar to class IB (BenC) and class III (NdoR) reductases, as both types contain FAD and plant-type [2Fe-2S] cluster-binding domains in a single protein, in contrast to other class II-type enzymes in which flavin (FAD) and [2Fe-2S] redox centers are found on separate proteins. MhpP exhibits low similarity with *Pseudomonas* sp. strain CF600 PH reductase (P5, 40 %) and *Acinetobacter* sp. ADP1 BenC (28 %). Phylogenetic analyses revealed that MhpP is closely related to other PH reductases (Fig. 1). MhpP can also oxidize NADPH using potassium ferricyanide, nitro blue tetrazolium, or cytochrome *c* as an artificial electron acceptor (Fig. 6). The activity of MhpP toward these artificial electron acceptors is in line with that of related enzymes such as BenC and NdoR, which can directly reduce these artificial electron acceptors in the presence of NAD(P)H (Haigler and Gibson 1990; Yamaguchi and Fujisawa 1978). Cytochrome *c* is a more suitable electron acceptor for MhpP. This observation is in line with the case of PHR from *Acinetobacter radioresistens,* in which cytochrome *c* is also more suitable than potassium ferricyanide and nitro blue tetrazolium (Pessione et al. 1999). These data indicate that *S. acidophilus* TPY MhpP is a novel NADPH-dependent reductase component of PH and contains FAD and a [2Fe-2S] cluster as cofactors.

Acknowledgments The study was supported by grants from the Natural Science Foundation of China (41306166), the National Key Basic Research Program of China ("973"-Program, 2015CB755903), the Natural Science Foundation of Fujian Province, China

(2016J05079), the Scientific Research Project of the Marine Public Welfare Industry of China (201205020), and the Xiamen South Ocean Research Center (13GZP002NF08).

Compliance with ethical standards No human participants and/or animals were involved in this work.

Conflict of interest The authors declare that they have no conflicts of interest.

References

Bradford MM (1976) A rapid and sensitive method for the quantitation of microgram quantities of protein utilizing the principle of protein-dye binding. Anal Biochem 72(1–2):248–254

Cafaro V, Scognamiglio R, Viggiani A, Izzo V, Passaro I, Notomista E, Piaz FD, Amoresano A, Casbarra A, Pucci P, Di Donato A (2002) Expression and purification of the recombinant subunits of toluene/o-xylene monooxygenase and reconstitution of the active complex. Eur J Biochem 269(22):5689–5699

Ceccarelli EA, Arakaki AK, Cortez N, Carrillo N (2004) Functional plasticity and catalytic efficiency in plant and bacterial ferredoxin-NADP (H) reductases. BBA-Proteins Proteom 1698(2):155–165

Chatwood LL, Muller J, Gross JD, Wagner G, Lippard SJ (2004) NMR structure of the flavin domain from soluble methane monooxygenase reductase from *Methylococcus capsulatus* (Bath). Biochemistry 43(38):11983–11991

Correll CC, Batie CJ, Ballou DP, Ludwig ML (1992) Phthalate dioxygenase reductase: a modular structure for electron transfer from pyridine nucleotides to [2Fe-2S]. Science 258(5088):1604–1610

Correll CC, Ludwig ML, Bruns CM, Karplus PA (1993) Structural prototypes for an extended family of flavoprotein reductases: comparison of phthalate dioxygenase reductase with ferredoxin reductase and ferredoxin. Protein Sci 2(12):2112–2133

Donadio G, Sarcinelli C, Pizzo E, Notomista E, Pezzella A, Di Cristo C, De Lise F, Di Donato A, Izzo V (2015) The toluene o-xylene monooxygenase enzymatic activity for the biosynthesis of aromatic antioxidants. PLoS One 10(4):e0124427

García LL, Rivas-Marín E, Floriano B, Bernhardt R, Ewen KM, Reyes-Ramírez F, Santero E (2011) ThnY is a ferredoxin reductase-like iron-sulfur flavoprotein that has evolved to function as a regulator of tetralin biodegradation gene expression. J Biol Chem 286(3):1709–1718

Guigliarelli B, Bertrand P (1999) Application of EPR spectroscopy to the structural and functional study of iron-sulfur proteins. Adv Inorg Chem 47(08):421–497

Haigler BE, Gibson DT (1990) Purification and properties of NADH-ferredoxinNAP reductase, a component of naphthalene dioxygenase from *Pseudomonas* sp. strain NCIB 9816. J Bacteriol 172(1):457–464

Jia Z, Xia H, Yuandong L, Jianshe L, Guanzhou Q (2007) Expression, purification, and characterization of a [Fe2S2] cluster containing ferredoxin from *Acidithiobacillus ferrooxidans*. Curr Microbiol 55(6):518–523

Karlsson A, Beharry ZM, Eby DM, Coulter ED, Neidle EL, Kurtz DM, Eklund H, Ramaswamy S (2002) X-ray crystal structure of benzoate 1, 2-dioxygenase reductase from *Acinetobacter* sp. strain ADP1. J Mol Biol 318(2):261–272

Karplus PA, Bruns CM (1994) Structure-function relations for ferredoxin reductase. J Bioenerg Biomembr 26(1):89–99

Karplus PA, Daniels MJ (1991) Atomic structure of ferredoxin-NADP+ reductase: prototype for a structurally novel flavoenzyme family. Science 251(4989):60–66

Kukor JJ, Olsen RH (1992) Complete nucleotide sequence of tbuD, the gene encoding phenol/cresol hydroxylase from *Pseudomonas pickettii* PKO1, and functional analysis of the encoded enzyme. J Bacteriol 174(20):6518–6526

Laura LG, Francisca RR, Eduardo S (2013) The ferredoxin ThnA3 negatively regulates tetralin biodegradation gene expression via ThnY, a ferredoxin reductase that functions as a regulator of the catabolic pathway. PLoS One 8(9):e73910

Li B, Chen Y, Liu Q, Hu S, Chen X (2011) Complete genome analysis of *Sulfobacillus acidophilus* strain TPY, isolated from a hydrothermal vent in the Pacific Ocean. J Bacteriol 193(19):5555–5556

Liu Y, Nesheim JC, Paulsen KE, Stankovich MT, Lipscomb JD (1997) Roles of the methane monooxygenase reductase component in the regulation of catalysis. Biochemistry 36(17):5223–5233

Mason JR, Cammack R (1992) The electron-transport proteins of hydroxylating bacterial dioxygenases. Annu Rev Microbiol 46(1):277–305

Merkx M, Kopp DA, Sazinsky MH, Blazyk JL, Mueller J, Lippard SJ (2001) Dioxygen activation and methane hydroxylation by soluble methane monooxygenase: a tale of two irons and three proteins. Angew Chem Int Ed 40(15):2782–2807

Nakajima T, Uchiyama H, Yagi O, Nakahara T (1992) Purification and properties of a soluble methane monooxygenase from *Methylocystis* sp. M. Biosci Biotechnol Biochem 56(5):736–740

Notomista E, Lahm A, Donato AD, Tramontano A (2003) Evolution of bacterial and archaeal multicomponent monooxygenases. J Mol Evol 56(4):435–445

Pessione E, Divari S, Griva E, Cavaletto M, Rossi GL, Gilardi G, Giunta C (1999) Phenol hydroxylase from *Acinetobacter radioresistens* is a multicomponent enzyme. Eur J Biochem 265(2):549–555

Powlowski J, Shingler V (1990) In vitro analysis of polypeptide requirements of multicomponent phenol hydroxylase from *Pseudomonas* sp. strain CF600. J Bacteriol 172(12):6834–6840

Qian H, Edlund UJ, Shingler V, Sethson I (1997) Solution structure of phenol hydroxylase protein component P2 determined by NMR spectroscopy. Biochemistry 36(3):495–504

Sazinsky MH, Lippard SJ (2006) Correlating structure with function in bacterial multicomponent monooxygenases and related diiron proteins. Acc Chem Res 37(45):558–566

Shingler V, Powlowski J, Marklund U (1992) Nucleotide sequence and functional analysis of the complete phenol/3,4-dimethylphenol catabolic pathway of *Pseudomonas* sp. strain CF600. J Bacteriol 174(3):711–724

Shinohara Y, Uchiyama H, Yagi O, Kusakabe I (1998) Purification and characterization of component B of a soluble methane monooxygenase from *Methylocystis* sp. M. J Ferment Bioeng 85(1):37–42

Shirabe K, Yubisui T, Nishino T, Takeshita M (1991) Role of cysteine residues in human NADH-cytochrome b5 reductase studied by site-directed mutagenesis. Cys-273 and Cys-283 are located close to the NADH-binding site but are not catalytically essential. J Biol Chem 266(12):7531–7536

Tinberg CE, Woon Ju S, Viviana I, Lippard SJ (2011) Multiple roles of component proteins in bacterial multicomponent monooxygenases: phenol hydroxylase and toluene/o-xylene monooxygenase from *Pseudomonas* sp. OX1. Biochemistry 50(11):1788–1798

Wang W, Liang AD, Lippard SJ (2015) Coupling oxygen consumption with hydrocarbon oxidation in bacterial multicomponent monooxygenases. Acc Chem Res 48(9):2632–2639

Whittington DA, Lippard SJ (2001) Crystal structures of the soluble methane monooxygenase hydroxylase from *Methylococcus capsulatus* (Bath) demonstrating geometrical variability at the dinuclear iron active site. J Am Chem Soc 123(5):827–838

Yamaguchi M, Fujisawa H (1978) Characterization of NADH-cytochrome c reductase, a component of benzoate 1, 2-dioxygenase system from *Pseudomonas arvilla* c-1. J Biol Chem 253(24):8848–8853

Zhou WG, Guo WB, Zhou HB, Chen XH (2016) Phenol degradation by *Sulfobacillus acidophilus* TPY via the meta-pathway. Microbiol Res 190:37–45